Asymmetric Responses in the Equatorial Pacific to Wind Forcing in OMIP2 Experiments: Role of Zonal Currents

Jin Li[1,2], Yongqiang Yu[1,2,*], De-Zheng Sun[3,*]

[1]National Key Laboratory of Earth System Numerical Modeling and Application, Institute of Atmospheric Physics, Chinese Academy of Sciences, Beiijing 100029, China.

[2]College of Earth and Planetary Sciences, University of Chinese Academy of Sciences, Beijing 100049, China.

[3]Nanjing-Helsinki Institute of Atmospheric and Earth System Sciences, Nanjing University Suzhou, Suzhou, Jiangsu 215163, China.

Corresponding author: Yongqiang Yu (yyq@lasg.iap.ac.cn) and De-Zheng Sun (dezheng.sun@nju.edu.cn)

Key Points:

- The asymmetric temperature response to zonal wind-stress forcing in the western Pacific is commonly underestimated by ocean models
- A generally weaker zonal currents in ocean models than in the observations is a cause of the underestimated asymmetric temperature response
- The weaker zonal current response in ocean models is linked to a less steep zonal tilt of the thermocline

Abstract

Numerical experiments from phase II of the Ocean Model Intercomparison Project (OMIP2) generally underestimate the asymmetric temperature response to interannual changes in the wind-stress over the equatorial western Pacific subsurface. Despite the knowledge that such a bias may be directly behind the general lack of asymmetry in model-simulated ENSO, its causes remain unknown. Here we report that a weaker response in the zonal currents to wind forcing in these models results in a biased response in the vertical motion which in turn causes weaker asymmetric temperature responses through the contribution of the vertical motion to the advective heating (dynamic heating). This finding underscores the critical importance of accurately modeling the zonal currents—a previously less noticed element in the modeling effort—to better capture the asymmetric responses in the tropical western Pacific to external wind forcing and thereby improving simulations of ENSO by coupled climate models.

Plain Language Summary

The responses of ocean dynamics to changes in atmospheric forcing plays a crucial role in simulating ENSO in fully-coupled climate models. This study utilizes simulations from stand-alone ocean models to show that ocean models underestimate temperature responses to atmospheric forcing in the western Pacific subsurface. The cause of this response is a weaker response in the zonal (west-east) ocean currents, which in turn leads to a biased response in vertical motion in the equatorial upper ocean and thereby a weaker dynamic heating. The weaker dynamic heating then results in the weakened temperature response. These findings highlight the need for accurately simulating zonal currents to improve simulation of ENSO by climate models, in particular its asymmetry.

1 Introduction

The El Niño-Southern Oscillation (ENSO) is the major interannual oscillation in the tropical Pacific (McPhaden et al., 2006; Timmermann et al., 2018). It arises from anomalous warming in the eastern tropical Pacific surface, which is amplified by oceanic zonal circulation driven by eastward wind-stress anomalies, a process known as the Bjerknes feedback (Bjerknes, 1969; Wyrtki, 1975). Accurate simulation of ENSO requires studying how oceanic processes respond to wind-stress (Hua & Yu, 2015).

A significant deviation in ENSO simulations by climate models is the temperature asymmetry over the western and eastern Pacific subsurface during El Niño and La Niña phases of ENSO (Zhang et al., 2009; Zhang & Sun, 2014; Zhao & Sun, 2022). This bias largely stems from the inadequate representation of nonlinear dynamic heating (NDH), especially its zonal component (Hayashi & Jin, 2017; Hayashi et al., 2020). Previous studies have primarily focused on investigating the sources of bias in ENSO asymmetry over the surface and subsurface of the eastern equatorial Pacific (An & Jin, 2004; Frauen & Dommenget, 2010; Carre et al., 2014; Zhao & Sun, 2022; Wang et al., 2023), leaving the western equatorial Pacific, particularly its subsurface, relatively underexplored. Since the equatorial undercurrent (EUC) forms in the western equatorial Pacific (Pedlosky, 1987; Pedlosky, 1991; Hu et al., 2015) and theories associated with ENSO cycles, such as recharge oscillator (Jin, 1997) and delayed oscillator (Suarez & Schopf, 1988), are established primarily based on western Pacific, it is crucial to study ENSO asymmetry in this region by investigating the ocean's dynamic responses to zonal wind-stress.

Here, to identify origins of the bias in temperature asymmetry related to oceanic dynamic processes and role of zonal currents in this bias, we utilize outputs from phase II of Ocean Model Intercomparison Project (OMIP2, Griffies et al., 2016) to diagnose the source of bias in asymmetric temperature responses to zonal wind-stress anomalies. The structure of this paper is as follows: Section 2 introduces the datasets and methods used for analysis. Section 3 presents the results, highlighting predominant ocean dynamic processes that cause the bias in asymmetric response of temperature in the western equatorial Pacific subsurface and section 4 provides a summary and discussion of the findings, along with suggestions for future research.

2 Data and Methods

2.1 Datasets

We obtained monthly ocean reanalysis variables (potential temperature, zonal, meridional, and vertical currents, sea surface zonal wind-stress) from the NCEP Global Ocean Data Assimilation System (GODAS) (Behringer et al., 1998), Simple Ocean Data Assimilation datasets (SODA, Carton & Giese, 2008) and GECCO versions 2 and 3 (Köhl, 2015; Köhl, 2020) from the Estimating the Circulation and Climate of the Ocean project. Details of the reanalysis datasets are provided in Table S1. OMIP2 offers simulation results from 15 Ocean-Sea ice coupled models, with an analysis period of 1980-2016 to ensure coverage across all datasets. Details of the ocean models are shown in Table S2. Ocean models from different institutes worldwide are primarily derived from a few core ocean model frameworks as shown in Table S2, such as POP, MOM and NEMO. To ensure clarity, we continue using the names of the climate models to represent their respective ocean components. Notably, positive and negative sign of vertical currents (zonal wind-stress) correspond to downwelling (eastward) and upwelling (westward), respectively. Subsurface zonal currents were validated using data from the Tropical Atmospheric Ocean (TAO) mooring array (2004-2016) (McPhaden, 1995).

2.2 Methods

The study focuses on investigating the source of bias of asymmetric response of temperature in ocean models. Monthly mean anomalies were used, with the seasonal cycle and warming trend removed. Bilinear interpolation was applied to unify the resolution onto a 1°×1° horizontal grid. The Niño-3 and Niño-4 regions were defined as 5°N-5°S, 150°W-90°W and 5°N-5°S, 160°E-150°W, respectively. The western and eastern equatorial Pacific subsurface regions (referred to as WEPS and EEPS) were (100 m-200 m, 2°S-2°N, 160°E-150°W) and (50 m-150 m, 2°S-2°N, 150°W-90°W), respectively.

Heat budget analysis is used to analyze the bias of dynamic heating terms in the ensemble-averaged model results compared to reanalysis datasets. The heat budget of the ocean subsurface layer is calculated using the temperature anomaly tendency equation as below (From Jin et al., 2003):

$$\begin{aligned} &\frac{\partial T'}{\partial t} = LDH + NDH + R \\ &LDH = -u'\frac{\partial \overline{T}}{\partial x} - v'\frac{\partial \overline{T}}{\partial y} - w'\frac{\partial \overline{T}}{\partial z} - \overline{u}\frac{\partial T'}{\partial x} - \overline{v}\frac{\partial T'}{\partial y} - \overline{w}\frac{\partial T'}{\partial z} \\ &NDH = -u'\frac{\partial T'}{\partial x} - v'\frac{\partial T'}{\partial y} - w'\frac{\partial T'}{\partial z} \end{aligned} \tag{1}$$

Here, is the potential temperature, and represent the zonal, meridional, and vertical velocities in the ocean, respectively; the overbar indicates the climatological mean, and the prime denotes anomalies. R represents sub-grid processes of heating and thermodynamic heating. The first and second terms on the right-hand side denote linear dynamic heating (referred to as LDH) and nonlinear dynamic heating (referred to as NDH), respectively, which can be calculated using the central difference approximation.

This study also adopts the composite analysis to characterize the asymmetric temperature responses to zonal wind-stress between warm (El Niño) and cold (La Niña) phases of ENSO. Warm (cold) phase of ENSO is defined as averaged temperature anomalies above 0.5°C (below -0.5°C) in the Niño-3 region (Zhang et al., 2009). In this paper, we attribute the asymmetric temperature response to the difference in amplitudes between El Niño and La Niña events over equatorial Pacific subsurface, same as the definition of temperature asymmetry in climate models because OMIP2 uses the same atmospheric forcing data to drive ocean models. We focus only on the one-way responses to isolate biases from ocean dynamics.

3 Results

We first evaluate the performance of standard deviation (STD) and ENSO asymmetry of temperature over Niño-3 (shown in Figure S1a and S1b), confirming that OMIP2 ocean models perform better in eastern equatorial Pacific surface compared to climate models from previous studies (Zhang and Sun, 2014; Zhao and Sun, 2022). As NDH along equatorial Pacific thermocline plays a crucial role in shaping ENSO temperature asymmetry (Hayashi et al., 2020), we then explore Pacific subsurface for the relationship between NDH (unit: °C/month) and asymmetric responses of temperature to zonal wind-stress (unit: °C) over WEPS (Figure 1, panels 1a and 1b) in comparison to EEPS (Figure 1, panels 1c and 1d) in stand-alone ocean models. NDH was divided into four components: three-dimensional NDH (referred to as NDH-Total, panels 1a and 1c) and zonal component of NDH (referred to as NDH-U, panels 1b and 1d), meridional and vertical component of NDH (referred to as NDH-V and NDH-W, respectively, depicted in Figure S3). As shown in Figs. 1a, 1c and S3, NDH-U is the dominant component of NDH, exhibiting a stronger heating rate than NDH-V and NDH-W. Neither NDH-U nor asymmetric temperature response in ocean models were underestimated compared with ocean reanalysis datasets over WEPS (as shown by the uniquely colored symbols in Figure 1a and Figure S2b), which aligns with the results derived from climate models (Zhao and Sun, 2022).

Additionally, Figure 1 illustrates that stronger asymmetric responses correlate with stronger positive NDH. NDH generally maintains positive over the equatorial Pacific, which could strengthen (weaken) El Nino (La Nina) events, in turn, leading to positive asymmetric temperature responses over eastern equatorial Pacific surface and subsurface (Jin et al., 2003; Hayashi and Jin, 2017; Figure 1c and 1d). This mechanism, however, seems invalid over WEPS in Figure 1a that stronger positive NDH corresponds to stronger negative asymmetric temperature responses. Thus, the bias of NDH-U may not directly drive the bias in negative asymmetric responses over WEPS in OMIP2 ocean models, warranting further investigation. Using Figure 1 as a starting point, one questions arise: why is asymmetric responses of temperature weaker in most ocean models from OMIP2 in WEPS?

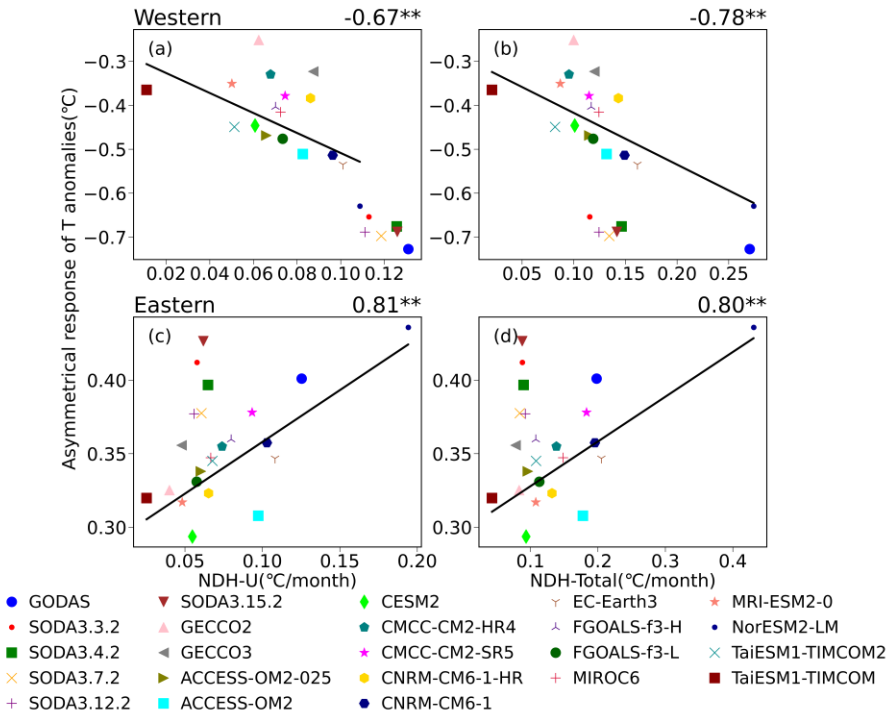

Figure 1. The relationship between nonlinear dynamic heating (NDH, unit: °C/month) and asymmetric responses of subsurface temperature anomalies (unit: °C) is examined among ocean models from OMIP2 over the western equatorial Pacific subsurface (a & b) and eastern equatorial Pacific subsurface (c & d). The left columns (a & c) depict the relationship with the zonal component of NDH, while the right columns (b & d) show the relationship with the three-dimensional NDH. Different symbols in unique colors represent distinct datasets, as indicated in the legends of the right panel of the figure. A black line represents the regression line, and the correlation coefficient is displayed in the upper right corner of each subgraph. Statistical significance is denoted by asterisks (* for 95% confidence level, ** for 99% confidence level), determined by standard Student's t-test.

To address this question, we conduct analysis of the ensemble heating rate of temperature anomalies during El Nino and La Nina events over WEPS. The terms for LDH and NDH (units: °C/month) are derived from Eq (1). Figure 2a illustrates that, on the one hand, as depicted in Figure 1a and Figure S3a, the NDH-U of OMIP2 models exhibits significantly weaker strength in both phases of ENSO compared to reanalysis datasets. On the other hand, what intrigues us is that the vertical velocity anomalies-induced LDH (hereafter: LDH-W′) in OMIP2 models are positively stronger during La Niña events than the ensemble of reanalysis datasets, weakening the asymmetric response of temperature. Additionally, positive NDH-U during La Niña events that can weaken the negative asymmetric temperature response, is notably weaker than LDH-W′. Therefore, it is confirmed that NDH-U is not the direct driving factor and stronger LDH-W′ during La Niña events emerges as the predominant factor contributing to the weaker asymmetric response of temperature in OMIP2 models.

Hua and Yu (2015) proposed that the oceanic dynamic asymmetric responses to wind-stress play a crucial role in ENSO asymmetry of temperature in the western Pacific. Results in

Figure 2a reveals the asymmetric heating rate LDH-W′ during two phases of ENSO in ocean reanalysis data, which corresponds to the conclusion from Hua and Yu (2015). LDH-W′, however, is less asymmetric in OMIP2 models and is dominated by vertical velocity anomalies in Eq (1). Further evaluation is needed to check the asymmetric response of vertical velocity anomalies. In Figure 2b, the vertical velocity anomalies are regressed against easterly and westerly anomalies for both reanalysis datasets and OMIP2 datasets. The last two bars represent the ensemble means of the reanalysis and OMIP2 datasets, respectively. It is evident that the response of vertical velocity anomalies to easterly anomalies are significantly stronger in the OMIP2 datasets compared to the reanalysis datasets. This bias then causes the stronger positive LDH-W′ during La Niña phase of ENSO (as illustrated in Figure 2a), consequently resulting in a weaker composited LDH-W′ in the OMIP2 results. These findings suggest that the weaker negative asymmetric responses of temperature over WEPS in OMIP2 is due to the less asymmetric LDH-W′. It is primarily exerted by a stronger response of downwelling to easterly anomalies with greater decline in thermocline than that in reanalysis datasets, which strengthen the positive LDH-W′ during La Niña phase.

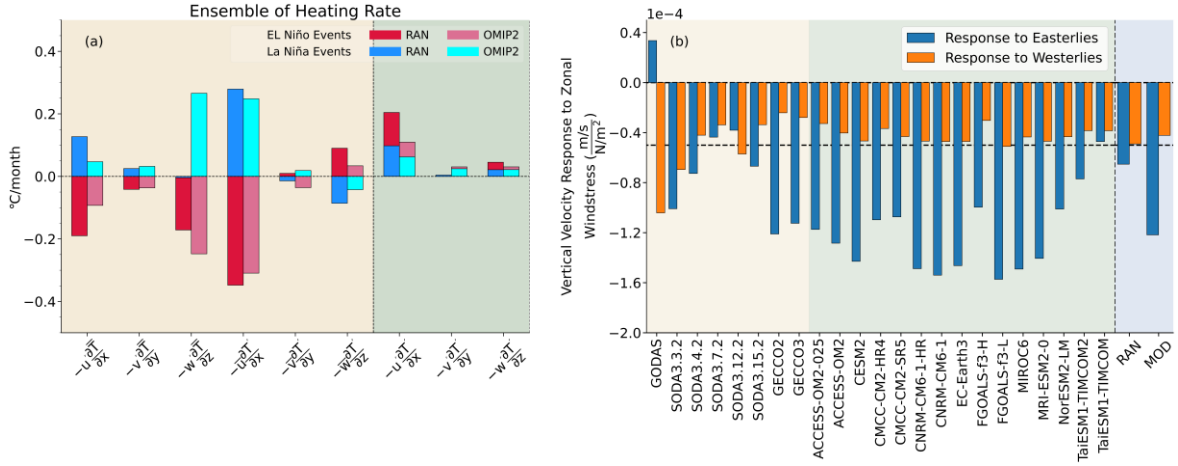

Figure 2. (a) Ensemble-averaged linear (brown shading) and nonlinear (green shading) heating rate terms in Eq(1) for temperature anomalies during El Niño and La Niña events over the western equatorial Pacific subsurface. (b) response (unit: (m/s)/(N/m²)) of vertical velocity anomalies averaged over western equatorial Pacific subsurface to easterly (blue bars) and westerly (orange bars) anomalies averaged over (2°S-2°N, 160°E-150°W) for reanalysis datasets (brown shading) and OMIP2 datasets (green shading), as well as the ensemble mean of reanalysis (RAN) and OMIP2 (MOD) datasets (blue shading).

Considering the Boussinesq approximation with character of ocean's incompressibility in ocean models, which ignores spatial-temporal density variations, the continuity equation degrades to:

$$-\left(\frac{\partial u'}{\partial x}+\frac{\partial v'}{\partial y}\right)=\frac{\partial w'}{\partial z} \tag{2}$$

where u′, v′, and w′ represent anomalies in the zonal, meridional, and vertical currents, respectively. Here, vertical velocity anomalies are the diagnostic variable and derived from zonal

and meridional currents through the continuity equation above. Further investigation is needed to confirm the primary source of the bias in vertical velocity anomalies. We first integrate these three terms from Eq (2) along depth to obtain vertical velocity induced by the zonal ($W_{u'}$) and meridional ($W_{v'}$) convergence, respectively:

$$\int_z^0 \frac{\partial w'}{\partial z} dz = \int_z^0 (-\frac{\partial u'}{\partial x}) dz + \int_z^0 (-\frac{\partial v'}{\partial y}) dz$$

$$W_{u'} = \int_z^0 (-\frac{\partial u'}{\partial x}) dz \quad (3)$$

$$W_{v'} = \int_z^0 (-\frac{\partial v'}{\partial y}) dz$$

then, averaging Eq (3) over WEPS and compare the OMIP2 ensemble mean with the reanalysis datasets ensemble mean to obtain the bias for each term as shown below:

$$[\frac{1}{V}\iiint_{WEPS} w' dxdydz]_{bias} = [\frac{1}{V}\iiint_{WEPS} W_{u'} dxdydz]_{bias} + [\frac{1}{V}\iiint_{WEPS} W_{v'} dxdydz]_{bias} \quad (4)$$

where V represents the volume of WEPS. We further divide the right-hand side of Eq (4) into two components: zonal and meridional components, to evaluate which term predominantly affect the bias of vertical velocity anomalies. Figure 3a depicts the relationship between vertical bias and zonal bias, meridional bias, and their combined effect during La Niña events, corresponding to Figure 2a. Primarily, the vertical bias is predominantly influenced by the combined effect of zonal and meridional biases, with correlation coefficient of 0.979 between them, as indicated by the red line in Figure 3a. Furthermore, the relative importance of zonal and meridional biases can be discerned by comparing the blue and black lines on Figure 3a. It is established that zonal bias, with a correlation coefficient of 0.700, holds greater significance compared to meridional bias, which has a correlation coefficient of -0.005. We use Figure 3b to examine the relationship between response of zonal current anomalies and response of vertical velocity anomalies during La Niña events, further comfirming the crucial role of zonal current anomalies. Thus, the biases in zonal current anomalies from OMIP2 results serve as the primary source of biases in vertical current anomalies.

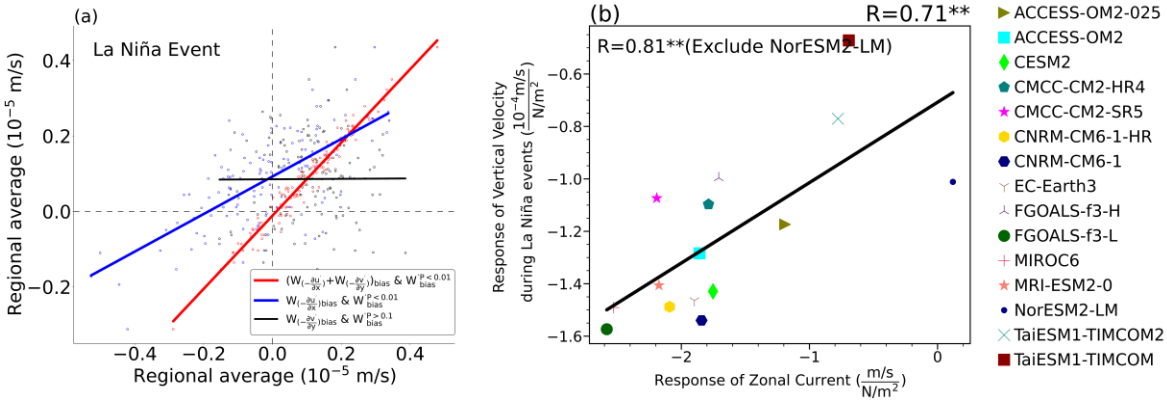

Figure 3. (a) Scatterplot depicting the relationship between the bias in vertical velocity anomalies due to horizontal currents (y-axis) and the overall bias in vertical velocity anomalies (x-axis) over the western equatorial Pacific subsurface during La Niña events. The biases (difference

between OMIP2 datasets and reanalysis ensemble datasets, unit: 10^{-5} m/s) are decomposed into contributions from horizontal, zonal, and meridional components, quantified by integrating the continuity equation (Eq. 2) along the depth. The regression lines for each component are shown in black, blue and red. Statistical significance, indicated in the legend, is determined by the standard Student's t-test. (b) Scatterplot illustrating the relationship between the response of zonal current anomalies to zonal wind-stress anomalies (unit: (m/s)/(N/m^2)) and the response of vertical velocity anomalies during La Niña events to zonal wind-stress anomalies (unit: (10^{-4}m/s)/(N/m^2)) in model results from OMIP2. The black line is the regression line, with the correlation coefficient (R) displayed in the upper-right corner. Statistical significance is denoted by asterisks (* for 95% confidence level, ** for 99% confidence level), determined by standard Student's t-test.

Subsequently, this study further explores the potential effect of biases in zonal current anomalies on mean state of ocean temperature. Figure 4a presents the time series of zonal current anomalies of observation, reanalysis, and model ensemble mean at a depth of 150 meters, along the equator at 170°W longitude (150 m, 170°W, EQ) from 2004 to 2015 (the details are shown in Figure S4). The baseline data is from the monthly TAO mooring array, with reanalysis and model results truncated to match the same extended time span as TAO. From Figure 4a, it is evident that the STD of zonal current anomalies is weaker in both the reanalysis (0.206 ± 0.037 m/s) and model results (0.167 ± 0.029 m/s) compared to TAO dataset (0.246 m/s). Notably, these reanalysis datasets do not assimilate current observations (Behringer et al., 1998, Carton & Giese, 2008), indicating that ocean currents, although regulated by observed temperature, salinity, and sea level, are underestimated. Meanwhile, the STD in the reanalysis datasets is slightly greater than that in the model results (as shown in Figure 4a and S6), confirming that the underestimation of asymmetric response of temperature arises from the models' inability to accurately simulate the subsurface zonal currents. The similar signal can also be found associated with the weaker negative response of zonal current anomalies in ocean models (-8.668 (m/s)/(N/m^2)) compared to that of reanalysis datasets (-9.531 (m/s)/(N/m^2)), as illustrated in the single-grid analysis in Figure 4a and at the location marked by the "X" in Figure S7. Furthermore, inspired by Wen et al (2014) which demonstrated the important role of thermocline variations in modulating ENSO evolutions, Figure 4b illustrates that the thermocline tilt, represented by gradient of depth of 20°C isotherm and with its bias shown in Figure S5 are proportional to the response of zonal current anomalies to zonal wind-stress anomalies among ocean models except NorESM2-LM. Although the ocean component of NorESM2-LM exhibits a more reasonable magnitude in the zonal current response at the "X" location (170°W, 150m) indicated in Figures 4a&S4, its spatial distribution over the WEPS region differs significantly from other datasets (Figure S7). This particular pattern suggests a cancellation of positive and negative values when averaged over the WEPS region. Seland et al. (2020) suggest that subsurface ocean biases in this model may be linked to the coarse ocean resolution and deficiencies in the parameterized processes. The bias of asymmetric temperature response has a pattern that resembles the bias of mean state of temperature over WEPS and EEPS (Figure S2a and S2b). This further emphasize the crucial role of rectification effect of ENSO on climate state of tropical ocean suggested in Sun et al (2014) through thermostat effect (Sun and Liu, 1996). And Sun and Liu (1996) revealed that responses of zonal currents are essential for modulating equilibrium of thermostat. Above all, zonal current response is tied to the thermocline mean state, warranting further study of their dynamical link.

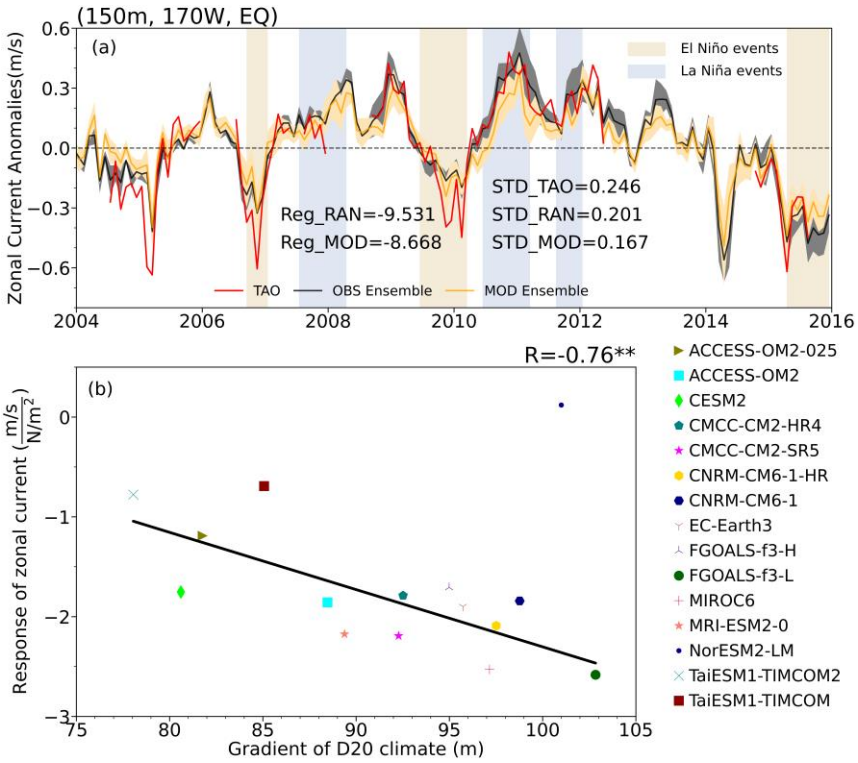

Figure 4. (a) The monthly time series of zonal current anomalies (in m/s) at 150 meters depth, 170°W longitude, and the Equator (EQ) for the period from 2004 to 2015 is presented, with the standard deviation of zonal currents anomalies from TAO, reanalysis and model datasets displayed in the lower right corner. The ensembled responses of zonal currents from reanalysis and model datasets at this site are shown in the middle. Data sources include the TAO mooring array (red), the ensemble-mean of reanalysis datasets (black), and the ensemble mean of OMIP2 models (orange). Gray and orange shading represent ±1 standard deviation for each dataset, respectively, illustrating the standard deviation and spread of different patterns. (b) Scatterplots illustrating the relationship between the gradient of the depth of 20°C isotherm in the mean state (unit: m) and the response of zonal current anomalies (averaged over 160°E-150°W, 2°S-2°N, 100m-200m) to zonal wind-stress anomalies (averaged over 160°E-150°W, 2°S-2°N). The gradient is defined as the depth difference between the western Pacific (160°E-150°W, 2°S-2°N) and the eastern Pacific (150°W-90°W, 2°S-2°N). The black line represents the regression line (excluding NorESM2-LM), with the correlation coefficient displayed in the upper right corner. Statistical significance is denoted by asterisks (* for 95% confidence level, ** for 99% confidence level), determined using the standard Student's t-test.

4 Conclusions and Discussions

In this work, we have identified the prevalent biases in asymmetric responses thermal and dynamical processes to zonal wind-stress at interannual timescales in stand-alone ocean models forced by JRA55 from OMIP2 over WEPS, especially the underestimated asymmetric temperature responses along the mean state of thermocline. Compared with results of reanalysis datasets, ocean models overestimate the response of vertical velocity anomalies to easterly anomalies. The resulting stronger linear dynamic heating induced by vertical velocity anomalies during cold phase of ENSO then lead to a weaker-negative asymmetric temperature responses to

external wind forcing. We have further used the continuity equation to diagnose the source of biases in the vertical velocity anomalies. The diagnosis has revealed that it is the bias in the zonal current anomalies that contribute most significantly to this bias over WEPS. Through comparing with TAO dataset and regression analysis, we have further revealed that standard deviation and responses of zonal current anomalies to zonal wind-stress anomalies in OMIP2 models are underestimated. This discrepancy is found to be linked to the weaker thermocline tilt in mean state. In summary, the answer to the question why the asymmetric responses of temperature are weaker in most ocean models from OMIP2 in WEPS may be phrased as follows:

> The primary reason is the stronger-than-observed response of vertical velocity anomalies to easterly anomalies, driven by biases in zonal current anomalies. This leads to a weaker LDH-W′ and diminishes the temperature response to zonal wind stress in OMIP2 models.

This study thus links the bias in asymmetric temperature responses to weaker zonal current responses, a factor often overlooked in previous research. The bias of asymmetric temperature responses has a pattern that resembles the bias of mean state of temperature over WEPS and EEPS, underscoring the role of rectification effect of ENSO on mean climate suggested in Sun et al (2014). The deviation of this effect in models' result depends on the bias in zonal current responses over WEPS. The strength of the response of zonal current to changes zonal wind-stress further plays a key role in the mean state of SST in the tropical Pacific Ocean through the dynamical thermostat mechanism (Sun and Liu, 1996).

Although existing theories have provided a perspective of describing the dynamics behind the relationship between response of zonal currents anomalies to zonal wind-stress anomalies and zonal tilt of the thermocline, further research is needed to pinpoint the source contributing to the bias in the zonal current response. To improve ocean models' ability to capturing ocean current responses to external forcing, advancements are needed in vertical mixing parameterizations (Fox-Kemper & Menemenlis, 2008). Traditionally, ocean models rely on empirical formulas to parameterize sub-grid processes, but their dependence on fixed parameters limits accuracy. With advances in machine learning, data-driven parameterization using observational or large eddy simulation data has emerged, improving efficiency and enhancing ocean dynamic simulations.

In summary, this study raises a crucial role of the zonal currents, in particular, their responses to external forcing in coupled atmosphere-ocean dynamics and modeling ENSO. To enhance the capability in simulating zonal currents in ocean models should be of a step of priority for further improving ENSO simulations by the fully-coupled climate models.

Acknowledgments

This study is jointly supported by National Natural Science Foundation of China (NSFC) (Grants 42130608 and Grants 42250710154) and the National Key Scientific and Technological Infrastructure project 'Earth System Numerical Simulation Facility' (EarthLab). And thanks to ICDC, CEN, University of Hamburg for data support.

Open Research

Data availability statement

The GODAS data are available from (https://www.psl.noaa.gov/data/gridded/data.godas.html). The SODA data are available from (https://www2.atmos.umd.edu/~ocean/index_files). The GECCO2 and GECCO2 data are available from (https://icdc.cen.uni-hamburg.de/thredds/catalog/ftpthredds/EASYInit/GECCO2/regular_1x1_grid/catalog.html) and (https://icdc.cen.uni-hamburg.de/thredds/catalog/ftpthredds/EASYInit/GECCO3/regular_1x1_grid/catalog.html). The TAO mooring array data are available from (https://www.pmel.noaa.gov/tao/drupal/disdel/). The CMIP6 datasets are available from (https://aims2.llnl.gov/search). The list of the CMIP6 models analyzed in the study can be found in Table S1.

References

An, S., & Jin, F. (2004). Nonlinearity and asymmetry of ENSO. *JOURNAL OF CLIMATE*, 17(12), 2399–2412. https://doi.org/10.1175/1520-0442(2004)017<2399:NAAOE>2.0.CO;2

Behringer, D. W., Ji, M., & Leetmaa, A. (1998). An Improved Coupled Model for ENSO Prediction and Implications for Ocean Initialization. Part I: The Ocean Data Assimilation System. *Monthly Weather Review*, 126(4), 1013–1021. https://doi.org/10.1175/1520-0493(1998)126<1013:AICMFE>2.0.CO;2

Bjerknes, J. (1969). Atmospheric teleconnections from the equatorial Pacific. *Monthly Weather Review*, 97(3), Article 3. https://doi.org/10.1175/1520-0493(1969)097<0163:ATFTEP>2.3.CO;2

Carre, M., Sachs, J., Purca, S., Schauer, A., Braconnot, P., Falcon, R., Julien, M., & Lavallee, D. (2014). Holocene history of ENSO variance and asymmetry in the eastern tropical Pacific. *Science*, 345(6200), Article 6200. https://doi.org/10.1126/science.1252220

Carton, J. A., & Giese, B. S. (2008). A Reanalysis of Ocean Climate Using Simple Ocean Data Assimilation (SODA). *Monthly Weather Review*, 136(8), 2999–3017. https://doi.org/10.1175/2007MWR1978.1

Fox-Kemper, B., & Menemenlis, D. (2008). Can large eddy simulation techniques improve mesoscale rich ocean models? In M. W. Hecht & H. Hasumi (Eds.), Geophysical Monograph Series (Vol. 177, pp. 319–337). American Geophysical Union. https://doi.org/10.1029/177GM19

Frauen, C., & Dommenget, D. (2010). El Nino and La Nina amplitude asymmetry caused by atmospheric feedbacks. *Geophysical Research Letters*, 37. https://doi.org/10.1029/2010GL044444

Griffies, S. M., Danabasoglu, G., Durack, P. J., Adcroft, A. J., Balaji, V., Böning, C. W., Chassignet, E. P., Curchitser, E., Deshayes, J., Drange, H., Fox-Kemper, B., Gleckler, P. J., Gregory, J. M., Haak, H., Hallberg, R. W., Heimbach, P., Hewitt, H. T., Holland, D. M., Ilyina, T., … Yeager, S. G. (2016). OMIP contribution to CMIP6: Experimental and diagnostic protocol for the physical component of the Ocean Model Intercomparison Project. *Geoscientific Model Development*, 9(9), 3231–3296. https://doi.org/10.5194/gmd-9-3231-2016

Hayashi, M., & Jin, F. (2017). Subsurface Nonlinear Dynamical Heating and ENSO Asymmetry. *Geophysical Research Letters*, 44(24), 12427–12435. https://doi.org/10.1002/2017GL075771

Hayashi, M., Jin, F.-F., & Stuecker, M. F. (2020). Dynamics for El Niño-La Niña asymmetry constrain equatorial-Pacific warming pattern. *Nature Communications*, 11(1), 4230. https://doi.org/10.1038/s41467-020-17983-y

Hu, D., Wu, L., Cai, W., Gupta, A. S., Ganachaud, A., Qiu, B., Gordon, A. L., Lin, X., Chen, Z., Hu, S., Wang, G., Wang, Q., Sprintall, J., Qu, T., Kashino, Y., Wang, F., & Kessler, W. S. (2015). Pacific western boundary currents and their roles in climate. *Nature*, 522(7556), 299–308. https://doi.org/10.1038/nature14504

Hua, L., & Yu, Y. (2015). The Asymmetry of Subsurface Temperature Anomalies Associated with ENSO in the Equatorial Western Pacific. *Atmospheric and Oceanic Science Letters*, 8(1), 23–28. https://doi.org/10.3878/AOSL20140067

Jin, F., An, S., Timmermann, A., & Zhao, J. (2003). Strong El Nino events and nonlinear dynamical heating. *Geophysical Research Letters*, 30(3). https://doi.org/10.1029/2002GL016356

Jin, F.-F. (1997). An Equatorial Ocean Recharge Paradigm for ENSO. Part I: Conceptual Model. *Journal of the Atmospheric Sciences*, 54(7), Article 7. https://doi.org/10.1175/1520-0469(1997)054<0811:AEORPF>2.0.CO;2

Köhl, A. (2015). Evaluation of the GECCO2 ocean synthesis: Transports of volume, heat and freshwater in the Atlantic. *Quarterly Journal of the Royal Meteorological Society*, 141(686), 166–181. https://doi.org/10.1002/qj.2347

Köhl, A. (2020). Evaluating the GECCO3 1948–2018 ocean synthesis–a configuration for initializing the MPI-ESM climate model. *Quarterly Journal of the Royal Meteorological Society*, 146(730), 2250-2273.

McPhaden, M. J. (1995). The Tropical Atmosphere Ocean Array Is Completed. *Bulletin of the American Meteorological Society*, 76(5), 739–744. https://doi.org/10.1175/1520-0477-76.5.739

McPhaden, M., Zebiak, S., & Glantz, M. (2006). ENSO as an integrating concept in Earth science. *Science*, 314(5806), 1740–1745. https://doi.org/10.1126/science.1132588

Pedlosky, J. (1987). An Inertial Theory of the Equatorial Undercurrent. *Journal of Physical Oceanography*, 17(11), 1978–1985. https://doi.org/10.1175/1520-0485(1987)017<1978:AITOTE>2.0.CO;2

Pedlosky, J. (1991). The Link between Western Boundary Currents and Equatorial Undercurrents. *Journal of Physical Oceanography*, 21(10), 1553–1558. https://doi.org/10.1175/1520-0485(1991)021<1553:TLBWBC>2.0.CO;2

Seland, Ø., Bentsen, M., Olivié, D., Toniazzo, T., Gjermundsen, A., Graff, L. S., Debernard, J. B., Gupta, A. K., He, Y.-C., Kirkevåg, A., Schwinger, J., Tjiputra, J., Aas, K. S., Bethke, I., Fan, Y., Griesfeller, J., Grini, A., Guo, C., Ilicak, M., … Schulz, M. (2020). Overview of the Norwegian Earth System Model (NorESM2) and key climate response of CMIP6 DECK, historical, and scenario simulations. Geoscientific Model Development, 13(12), 6165–6200. https://doi.org/10.5194/gmd-13-6165-2020

Suarez, M. J., & Schopf, P. S. (1988). A Delayed Action Oscillator for ENSO. *Journal of the Atmospheric Sciences*, 45(21), Article 21. https://doi.org/10.1175/1520-0469(1988)045<3283:ADAOFE>2.0.CO;2

Sun, D., Zhang, T., Sun, Y., & Yu, Y. (2014). Rectification of El Nino-Southern Oscillation into Climate Anomalies of Decadal and Longer Time Scales: Results from Forced Ocean GCM Experiments. *Journal of Climate*, 27(7), Article 7. https://doi.org/10.1175/JCLI-D-13-00390.1

Sun, D.-Z., & Liu, Z. (1996). Dynamic Ocean-Atmosphere Coupling: A Thermostat for the Tropics. *Science*, 272(5265), Article 5265. https://doi.org/10.1126/science.272.5265.1148

Timmermann, A., An, S., Kug, J., Jin, F., Cai, W., Capotondi, A., Cobb, K., Lengaigne, M., McPhaden, M., Stuecker, M., Stein, K., Wittenberg, A., Yun, K., Bayr, T., Chen, H., Chikamoto, Y., Dewitte, B., Dommenget, D., Grothe, P., … Zhang, X. (2018). El Nino-Southern Oscillation complexity. *Nature*, 559(7715), 535–545. https://doi.org/10.1038/s41586-018-0252-6

Wang, C., Wang, S., Jing, Z., Geng, T., Wang, H., & Wu, L. (2023). Equatorial Submesoscale Eddies Contribute to the Asymmetry in ENSO Amplitude. *Geophysical Research Letters*, 50(5), e2022GL101352. https://doi.org/10.1029/2022GL101352

Wen, C., Kumar, A., Xue, Y., & McPhaden, M. J. (2014). Changes in Tropical Pacific Thermocline Depth and Their Relationship to ENSO after 1999. Journal of Climate, 27(19), 7230–7249. https://doi.org/10.1175/JCLI-D-13-00518.1

Wyrtki, K. (1975). El Niño—The Dynamic Response of the Equatorial Pacific Oceanto Atmospheric Forcing. *Journal of Physical Oceanography*, 5(4), Article 4. https://doi.org/10.1175/1520-0485(1975)005<0572:ENTDRO>2.0.CO;2

Zhang, T., & Sun, D. (2014). ENSO Asymmetry in CMIP5 Models. *Journal of Climate*, 27(11), Article 11. https://doi.org/10.1175/JCLI-D-13-00454.1

Zhang, T., Sun, D., Neale, R., & Rasch, P. (2009). An Evaluation of ENSO Asymmetry in the Community Climate System Models: A View from the Subsurface. *Journal of Climate*, 22(22), 5933–5961. https://doi.org/10.1175/2009JCLI2933.1

Zhao, Y., & Sun, D.-Z. (2022). ENSO Asymmetry in CMIP6 Models. *Journal of Climate*, 35(17), 5555–5572. https://doi.org/10.1175/JCLI-D-21-0835.1

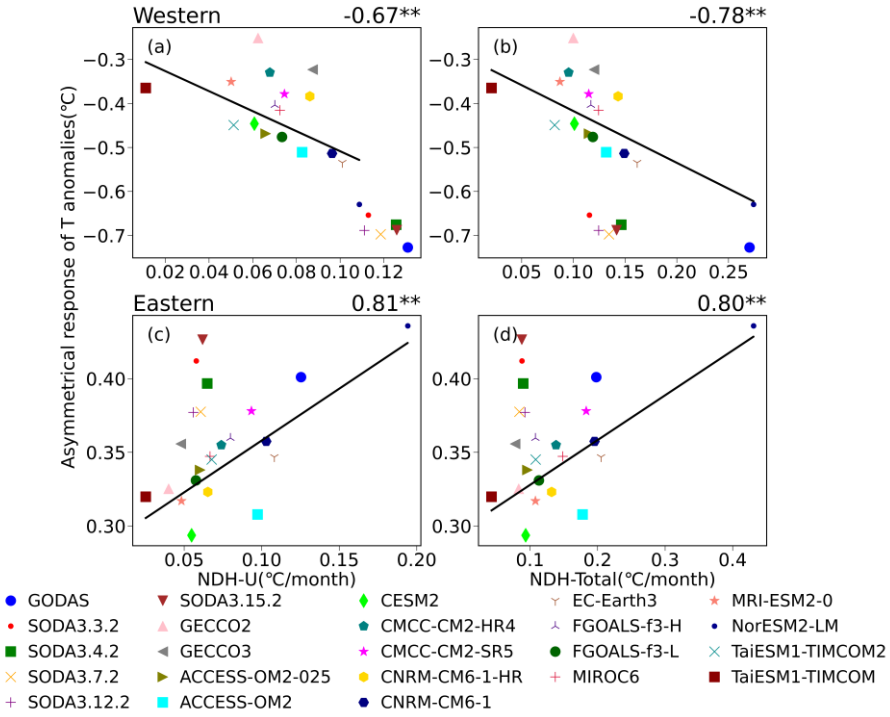

Figure 1. The relationship between Nonlinear Dynamic Heating (NDH, unit: °C/month) and subsurface asymmetric response of T anomalies (unit: °C) is examined over the western equatorial Pacific subsurface (a & b) and eastern equatorial Pacific subsurface (c & d). The left columns (a & c) depict the relationship with the zonal component of NDH, while the right columns (b & d) show the relationship with the three-dimensional NDH. Different symbols in unique colors represent distinct datasets, as indicated in the legends of the right panel of the figure. A black line represents the regression line, and the correlation coefficient is displayed in the upper right corner of each subgraph. Statistical significance is denoted by asterisks (* for 95% confidence level, ** for 99% confidence level), determined by standard Student's t-test.

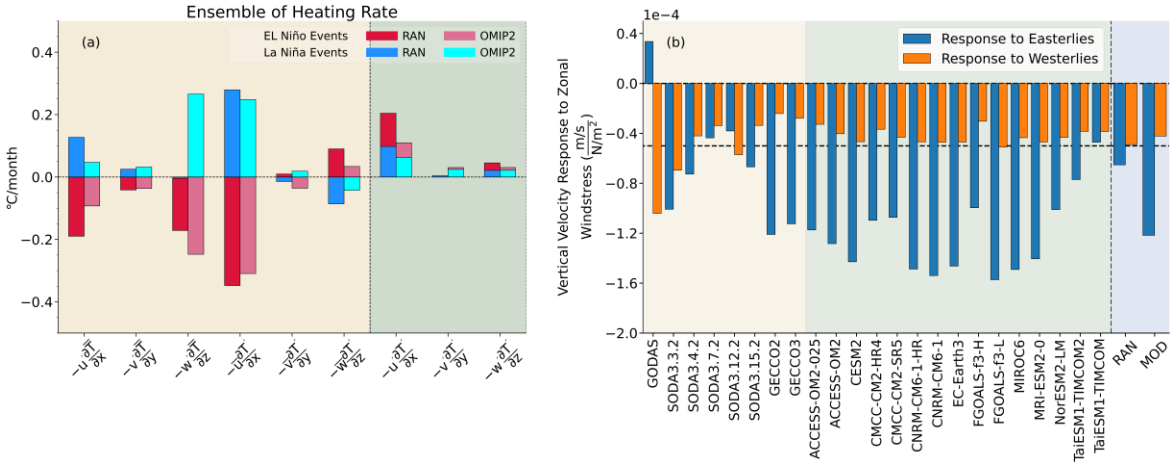

Figure 2. (a) Ensemble-averaged linear (brown shading) and nonlinear (green shading) heating rate terms in Eq(1) for temperature anomalies during El Niño and La Niña events over the western equatorial Pacific subsurface. (b) response (unit: (m/s)/(N/m²)) of vertical velocity anomalies averaged over western equatorial Pacific subsurface to easterly (blue bars) and westerly (orange bars) anomalies averaged over (2°S-2°N, 160°E-150°W) for reanalysis datasets (brown shading) and OMIP2 datasets (green shading), as well as the ensemble mean of reanalysis (RAN) and OMIP2 (MOD) datasets (blue shading).

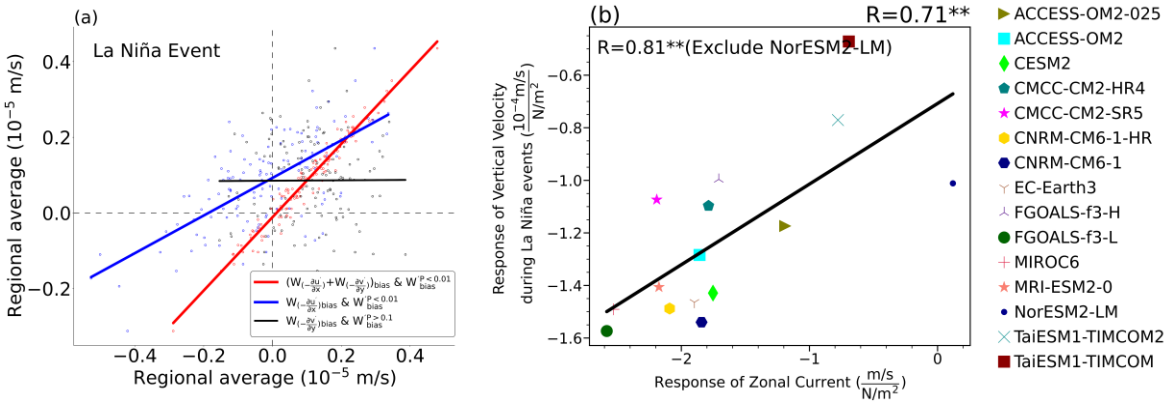

Figure 3. (a) Scatterplot depicting the relationship between the bias in vertical velocity anomalies due to horizontal currents (y-axis) and the overall bias in vertical velocity anomalies (x-axis) over the western equatorial Pacific subsurface during La Niña events. The biases (difference between OMIP2 datasets and reanalysis ensemble datasets, unit: $10^{-}5$ m/s) are decomposed into contributions from horizontal, zonal, and meridional components, quantified by integrating the continuity equation (Eq. 2) along the depth. The regression lines for each component are shown in black, blue and red. Statistical significance, indicated in the legend, is determined by the standard Student's t-test. (b) Scatterplot illustrating the relationship between the response of zonal current anomalies to zonal wind-stress anomalies (unit: (m/s)/(N/m2)) and the response of vertical velocity anomalies during La Niña events to zonal wind-stress anomalies (unit: (10-4m/s)/(N/m2)) in model results from OMIP2. The black line is the regression line, with the correlation coefficient (R) displayed in the upper-right corner. Statistical significance is denoted by asterisks (* for 95% confidence level, ** for 99% confidence level), determined by standard Student's t-test.

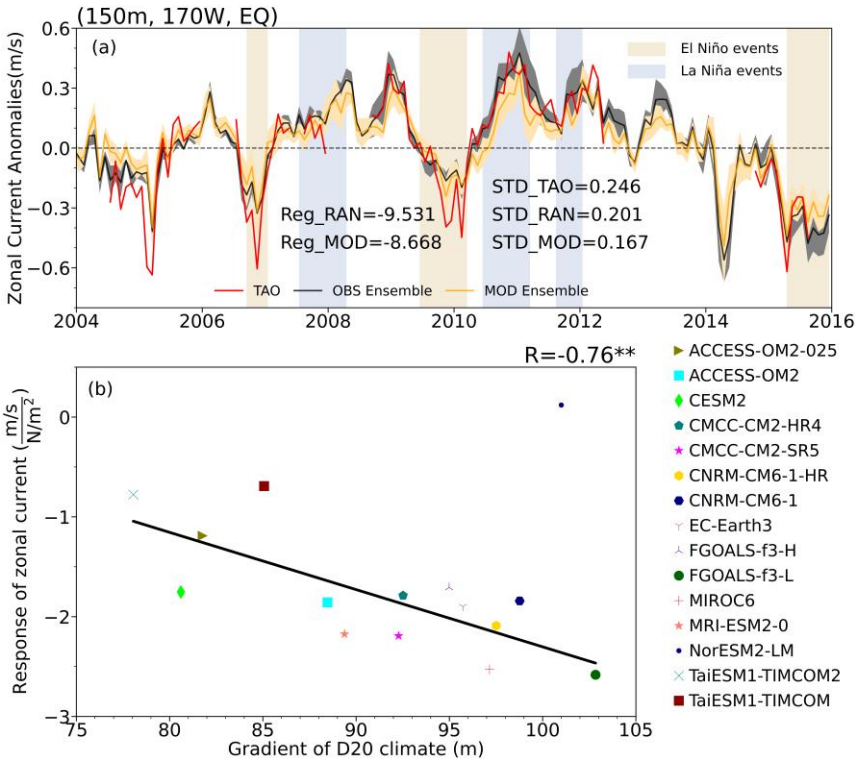

Figure 4. (a) The monthly time series of zonal current anomalies (in m/s) at 150 meters depth, 170°W longitude, and the Equator (EQ) for the period from 2004 to 2015 is presented, with the standard deviation of zonal currents anomalies from TAO, reanalysis and model datasets displayed in the lower right corner. The ensembled responses of zonal currents from reanalysis and model datasets at this site are shown in the middle. Data sources include the TAO mooring array (red), the ensemble-mean of reanalysis datasets (black), and the ensemble mean of OMIP2 models (orange). Gray and orange shading represent ±1 standard deviation for each dataset, respectively, illustrating the standard deviation and spread of different patterns. (b) Scatterplots illustrating the relationship between the gradient of the depth of 20°C isotherm in the mean state (unit: m) and the response of zonal current anomalies (averaged over 160°E-150°W, 2°S-2°N, 100m-200m) to zonal wind-stress anomalies (averaged over 160°E-150°W, 2°S-2°N). The gradient is defined as the depth difference between the western Pacific (160°E-150°W, 2°S-2°N) and the eastern Pacific (150°W-90°W, 2°S-2°N). The black line represents the regression line (excluding NorESM2-LM), with the correlation coefficient displayed in the upper right corner. Statistical significance is denoted by asterisks (* for 95% confidence level, ** for 99% confidence level), determined using the standard Student's t-test.